How to cite: *Angew. Chem. Int. Ed.* **2020**, *59*, 19329–19337
International Edition: doi.org/10.1002/anie.202007715
German Edition: doi.org/10.1002/ange.202007715

NMR Spectroscopy Hot Paper

Enabling NMR Studies of High Molecular Weight Systems Without the Need for Deuteration: The XL-ALSOFAST Experiment with Delayed Decoupling

*Philip Rößler, Daniel Mathieu, and Alvar D. Gossert**

Abstract: *Current biological research increasingly focusses on large human proteins and their complexes. Such proteins are difficult to study by NMR spectroscopy because they often can only be produced in higher eukaryotic expression systems, where deuteration is hardly feasible. Here, we present the XL-ALSOFAST-[^{13}C,^{1}H]-HMQC experiment with much improved sensitivity for fully protonated high molecular weight proteins. For the tested systems ranging from 100 to 240 kDa in size, 3-fold higher sensitivity was obtained on average for fast relaxing signals compared to current state-of-the-art experiments. In the XL-ALSOFAST approach, non-observed magnetisation is optimally exploited and transverse relaxation is minimized by the newly introduced concept of delayed decoupling. The combination of high sensitivity and superior artefact suppression makes it ideal for studying inherently unstable membrane proteins or for analysing therapeutic antibodies at natural ^{13}C abundance. The XL-ALSOFAST and delayed decoupling will therefore expand the range of biomolecular systems accessible to NMR spectroscopy.*

Introduction

In the past decade structural biology has provided a wealth of insights into human health and disease at the molecular level. The relevant proteins under investigation are often membrane proteins and protein complexes which previously were very difficult to produce in bacterial cells. Such proteins can nowadays be studied directly, because methods have been developed to produce them in large amounts in eukaryotic expression hosts where the required folding machinery is present and protein complexes are correctly assembled.[1–3] However, these newly established biomolecular systems are not readily accessible to nuclear magnetic resonance (NMR) studies. NMR spectroscopy is a powerful tool for the characterisation of biomolecules and biomolecular complexes at atomic resolution in solution and could provide valuable complementary information to electron microscopy data or crystal structures. However, being a highly diverse technique for small proteins up to 25 kDa, NMR spectroscopy drastically suffers from size limitations: when working with larger proteins measurement times become very long and the information content of the NMR method is highly reduced.[4,5] This especially applies to proteins which are difficult to produce in deuterated form, like proteins expressed in eukaryotic expression systems.

In order to illustrate the problems imposed by large protonated samples and to later demonstrate the broad applicability and the advantages of the presented approach, we use two representative examples of challenging applications: membrane proteins and therapeutic antibodies. These cover the diverse realms of fundamental biological and applied pharmaceutical research.

For transmembrane receptors, which comprise the largest class of drug targets[6–14] NMR has provided most important insights into their function and dynamics. For NMR studies in solution these membrane proteins must be solubilized in membrane mimics like detergent micelles or nanodiscs,[15–17] which increase the molecular weight of the particles under study by 80–150 kDa. The sensitivity of NMR is very low with particles of this size and therefore measurement times even for simple spectra typically are in the range of a day, and therefore often only stabilized surrogates of human proteins are amenable to NMR studies.[10,11]

In the case of therapeutic antibodies (150 kDa) NMR provides important analytical data on formulated drug preparations, where the integrity of the antibody in terms of proper fold, degradation, oxidative changes etc. can be characterized in a single spectrum.[18–21] Also here, measurements of a single sample can take a full day on a high field instrument.

There has been great progress in the past in extending the size range of NMR, and particles up to sizes of a Mega-Dalton have been studied.[22,23] These successes rely on a combination of isotope labelling techniques, namely deuteration,[24] and TROSY-type NMR experiments on amide or methyl groups.[25,26] Unfortunately, many higher eukaryotic expression systems do currently not allow the production of deuterated samples or are not able to achieve the necessary

[*] P. Rößler, A. D. Gossert
Institute of Molecular Biology and Biophysics, Department of Biology and Biomolecular NMR Spectroscopy Platform, Department of Biology, ETH Zürich
Otto-Stern-Weg 5, 8093 Zürich (Switzerland)
E-mail: alvar.gossert@biol.ethz.ch
D. Mathieu
Bruker BioSpin GmbH
Silberstreifen 4, 76287 Rheinstetten (Germany)
Supporting information and the ORCID identification number(s) for the author(s) of this article can be found under https://doi.org/10.1002/anie.202007715.

high levels of deuterium incorporation.[27] In a few cases deuteration has been successfully performed in insect cells with incorporation levels of up to 60–75 %[7,27–30] but no successful production of deuterated protein from mammalian cell lines has been reported yet. This also applies to the two examples discussed here, integral membrane proteins and therapeutic antibodies, which are produced in human embryonic kidney cell lines (HEK293) and Chinese hamster ovary cell lines (CHO) in non-deuterated form. In a non-deuterated background TROSY techniques are much less effective, because the NMR signals are already strongly broadened by dipolar relaxation.[31] The inability to produce deuterated proteins in these higher expression systems therefore limits NMR applications to a subset of small proteins.

Currently, the best-performing NMR experiments on large protonated particles are based on SOFAST-[^{13}C,^{1}H]-HMQC pulse sequences.[6–8,11] The success of this approach is based on (i) recording signals of methyl groups, (ii) using HMQC-type pulse sequences and (iii) the SOFAST scheme. (i) Methyl groups have intrinsically high sensitivity due to the multiplicity of three, the high rotation rate about the methyl group and the typically high flexibility of the long side chains. (ii) Using an HMQC experiment the methyl-TROSY effect is exploited,[26,32] such that fast and slowly relaxing components are not mixed during the pulse sequence and therefore preserving sharp signals. (iii) The SOFAST (band-Selective Optimized-Flip-Angle Short-Transient) technique was originally developed for speedy recording of NMR experiments, by shortening the recovery delay.[33] For large proteins, the SOFAST approach improves sensitivity by only exciting part of the spectrum, such that the non-observed spins remain at equilibrium magnetisation and help the observed spins to quickly regain equilibrium by cross relaxation, which is extremely efficient in large protonated proteins. If the protein was fully saturated after the pulse sequence, much slower spin-lattice relaxation processes would apply. Although the SOFAST approach should not saturate the solvent, samples of large proteins are typically buffer-exchanged into D_2O-based buffers in order not to transfer potential saturation of water magnetisation into the protein, and to increase the overall deuteration level. However, even with all these optimizations, it takes several hours to obtain high-quality spectra of for example, a 50 μM sample of a G protein-coupled receptor (GPCR), and it is thus not possible to work with unstable samples.

The second requirement besides high sensitivity, often encountered for such samples is efficient suppression of artefactual signals: for membrane proteins these are detergents at typically 100-fold concentration of the protein, for antibodies these are excipients and the 100-fold stronger signals of the unlabelled moieties, as antibodies are measured with natural isotope abundance. In practice high-quality spectra can only be obtained with a gradient selection (gs) procedure.[34] This, however, also leads to important losses of signal, because the pulse sequence needs to be lengthened by an additional INEPT step to record the orthogonal signal component and a spin echo for gradient decoding.[35,36] For large protonated particles the losses due to relaxation during this additional element are often more important than the gain. Therefore, it is common practice to just record a regular HMQC and sacrificing the losses due to gradient selection. However, even with gradient selection, the signal of some contaminants is so intense that additional dedicated suppression schemes are needed[37] which lead to additional losses of the protein signal due to relaxation.

With this background we sought to develop an experiment for large protonated biomolecules, which is more sensitive than current approaches, and still takes into account the requirements for artefact suppression and ideally does not require deuterated buffers. This would potentially enable studies on unstable proteins or proteins that are only available at low concentrations.

Our approach leading to the new XL-ALSOFAST experiment is tripartite: First, we replace the SOFAST approach with the less known ALSOFAST scheme.[38,39] Second, we introduce the concept of "delayed decoupling" in order to optimize the ALSOFAST pulse sequence for minimal relaxation losses. And third, we improve artefact suppression by combining gradient selection with alignment of all unwanted magnetisation along the $+z$-axis, where it does not contribute to the NMR signal.

The ALSOFAST experiment is derived from the SOFAST experiment, where selective pulses are used for excitation of the spins of interest. With large proteins one typically focuses on a subset of signals (e.g. one amino acid type is labelled or only well-dispersed methyl groups are recorded), since recording all signals inevitably would lead to complete overcrowding of spectra. Therefore, one might only want to observe a dozen of methyl groups. In a methyl SOFAST-[^{13}C,^{1}H]-HMQC, the upfield region of the spectrum is excited and all other spins, including the solvent, stay at equilibrium along the static B_0 field. While this is achieved in the SOFAST

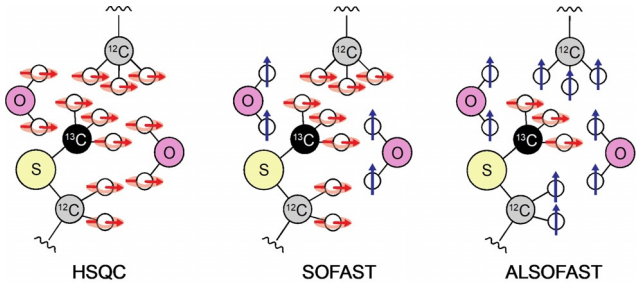

Figure 1. Highly selective excitation with the ALSOFAST experiment. The magnetisation of nuclei in a protein sample are shown after completion of different pulse sequences, identified below each scheme. The aim is to record the signal of the central methyl group, which is ^{13}C labelled (black). Depending on the pulse sequence, non-observed magnetisation of nuclei in the vicinity ends up in the transverse plane (red arrows) or aligned along the $+z$ axis (blue arrows). The latter will contribute to fast relaxation of the observed nuclei towards equilibrium and thus to higher sensitivity. The standard HSQC experiments result in the excitation of the full sample. Excitation becomes more selective with the SOFAST scheme where only the upfield region is excited. However, while the magnetisation of the solvent stays in equilibrium, large portions of the protein and for example, buffer or detergent signals will be excited. The most selective excitation is achieved using the ALSOFAST scheme, which is based on isotope editing.

scheme by selective pulses, ALSOFAST makes use of only hard pulses in an isotope editing element[38] and ultimately yields a more selective excitation (Figure 1).

Using the ALSOFAST experiment as a basis we developed the XL-ALSOFAST experiment which results in 2–3-fold higher sensitivity for large protonated biomolecules and allows studying challenging and unstable samples. In addition, it can cope much better with strong background signals than the original experiment.

Results and Discussion

In this study, we developed the XL-ALSOFAST-HMQC (XL: eXtra Large) for studying fully protonated high molecular weight systems that are strongly suffering from relaxation (Figure 2A). Our first goal was to minimize relaxation losses during the pulse sequence by shortening it. However, the duration of the pulse sequence is dictated by

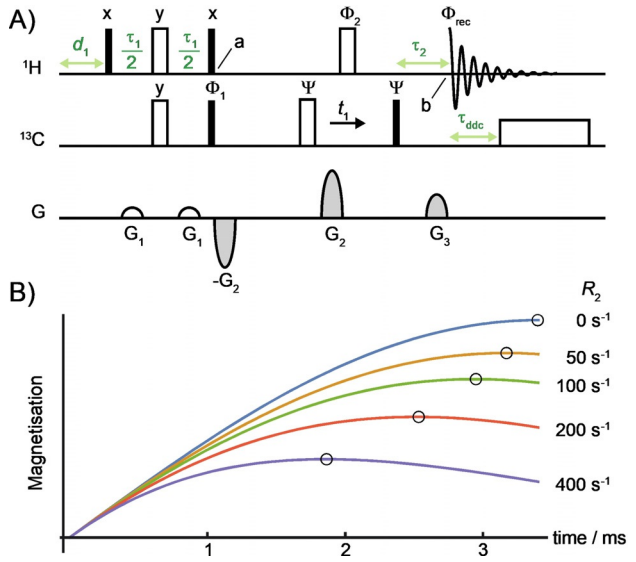

Figure 2. (A) Pulse sequence of the XL-ALSOFAST-[^{13}C,^{1}H]-HMQC with gradient selection (gs). 90° and 180° pulses are shown as filled and empty rectangles, respectively, with phases indicated on top. The forward and backward INEPT delays are τ_1 and τ_2, respectively and the delay before decoupling (τ_{ddc}) is calculated from $\tau_{ddc}=1/2J_{CH}-\tau_2$. Gradients were of 500 µs length and fulfil the relation $2G_2/3.97=G_3$. Phase sensitive spectra are obtained using the echo-antiecho method with ψ: x,x, $-x,-x$ and simultaneous inversion of gradients G_2 and G_3. Phase cycling is used as Φ_1: $x,-x$; Φ_2: x,x,x,x, $-x,-x,-x,-x$, y,y,y,y, $-y,-y,-y,-y$; Φ_{rec}: $x,-x,-x,x$, $x,-x,-x,x$, $-x,x,x,-x$, $-x,x,x,-x$. See supplementary material for the full pulse program. (B) Calculated magnetisation transfer during an INEPT delay. The transfer is following a sine curve (see equation 1) with maximal transfer after 3.4 ms for CH moieties ($^1J_{CH}=147$ Hz). The optimal transfer time given by the maximum of the transfer curve (marked by circles) is decreasing with increasing relaxation rates.

INEPT (insensitive nuclei enhanced by polarization transfer) delays, and shortening them will always lead to reduced magnetisation transfer. We therefore developed novel approaches to minimize these losses. Two different strategies were developed for the forward (H→C) and the reverse (C→H) INEPT, respectively.

Shortening of the forward INEPT delay while preserving non-transferred magnetisation for the next scan

Generally, magnetisation is transferred during an INEPT transfer between one nucleus (H) to another coupled nucleus (C). Transfer efficiency follows the form of a sine curve attenuated by an exponential function describing transverse relaxation [Eq. (1)].

$$M_C(\tau) = \sin(\pi J_{CH}\tau)\cdot\exp(-R_2\tau), \quad (1)$$

where J_{CH} is the scalar coupling between C and H nuclei, τ the INEPT delay and R_2 is the transverse relaxation rate of the H nucleus. Equation (1) is plotted in Figure 2B for different values of the transverse relaxation rate. The maxima of the transfer efficiency curves for high R_2 relaxation rates precede the length of the full INEPT delay ($=1/2J$, calculated from Equation (1) by neglecting R_2). Therefore, it is straightforward to reduce the INEPT delay for large proteins to the optimal value depending on R_2.[40] By doing so, part of the H magnetisation is not transferred ($\cos(\pi J_{CH}\tau)\cdot\exp(-R_2\tau)$) and is typically lost. However, using the ALSOFAST scheme, the non-transferred magnetisation is flipped along the z-axis by the $90°_x$ pulse at the end of the forward INEPT element and can thus be used in the subsequent scan. The amount of magnetisation carried over into the next scan depends on the length of the recovery delay d_1, in an analogous manner as Ernst angle excitation.[41] Therefore, d_1 must be optimised together with the length of the forward INEPT delay to achieve the best possible improvement of the experiment.

Note that this type of "lossless" shortening of the forward INEPT is not possible with the standard SOFAST approach: First, the shaped pulse for excitation has a typical duration of 2.4 ms and together with the following gradient doesn't leave much room for shortening of the INEPT delay and second, the excited spins are fully saturated without the possibility of recovering non-transferred magnetisation in the next scan.

The $90°_x$ pulse at point a in Figure 2A in the XL-ALSOFAST sequence therefore is central to its performance and, as will be discussed later, also for artefact suppression. However, this 90° pulse leads to mixing of spin states of the methyl group and therefore, the methyl TROSY effect is only fully exploited from this point onwards in the NMR experiment. For fully protonated proteins, however, the TROSY effect is not highly relevant. Overall therefore the advantages of using this selective excitation scheme prevail, as it allows to flip all non-observed magnetisation along the z-axis.

The water signal represents a special case of non-observed magnetisation. In theory it follows the magnetisation path of other non-observed magnetisation and ends up fully aligned along the $+z$-axis at the end of the experiment (point b in Figure 2A), such that it can contribute to fast longitudinal relaxation of the biomolecule towards an equilibrium state. However, for water there are losses due to radiation damping, which we try to mitigate by the use of gradients. In this way we

measured that 80% of the original water magnetisation is conserved along the $+z$-axis at steady state (Figure S1). Therefore, there is no need for transferring the protein under study into perdeuterated buffer, which saves work time and avoids the losses concomitant with dialysis or repeated concentration steps.

In summary, the first INEPT element in the XL-ALSOFAST has two functions. First, it allows surgically precise excitation and transfer of magnetisation that shall be observed, while keeping all non-observed magnetisation along the z-axis. Therefore, all non-observed magnetisation in the vicinity—be it detergents, water, or other methyl groups with similar chemical shift—will contribute to more efficient longitudinal relaxation of the spins of interest and ultimately to higher signal. Second, this special INEPT element allows shortening of the INEPT delay for reducing relaxation losses, while preserving non-transferred magnetisation for the next scan.

Delayed decoupling (ddc) allows shortening of the reverse INEPT delay without losses

The reverse INEPT must be optimized in a different way. Reducing the length of the INEPT delay is again of great benefit for fast relaxing signals (Figure 3, blue schemes). However, here non-transferred magnetisation is lost as soon as heteronuclear decoupling is started. For this reason, we introduce the concept of "delayed decoupling" (ddc; Figure 3, red schemes). In delayed decoupling, the reverse INEPT delay is shortened and acquisition is started at $\tau_2 < 1/2J_{CH}$ (e.g. $\tau_2 = 1.4$ ms, Figure 2A at point b), but decoupling is only initiated after $1/2J_{CH}$ (e.g. 3.4 ms) when the theoretical maximum of magnetisation transfer is reached. Hence, decoupling is delayed with respect to the start of signal acquisition, specifically by $\tau_{ddc} = 1/2J - \tau_2$. The resulting free induction decay (FID) has a characteristic shape: there is an initial increase while magnetisation is still transferred and once decoupling is started the monotonous decay of the signal according to R_2 is visible. With delayed decoupling, the signal intensity in the time domain is higher and it persists for a longer time. Note that the noise level for all three signals in Figure 3 is identical. After Fourier transform this results in a sharper signal with higher intensity (Figure 3C).

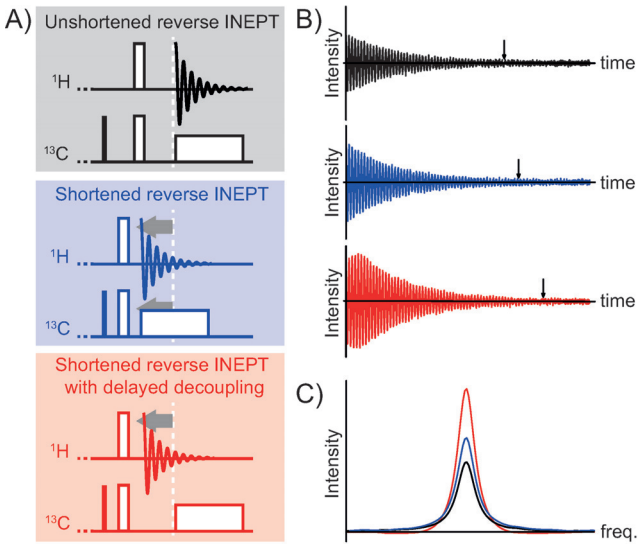

Figure 3. Effect of delayed decoupling on the NMR signal. (A) Pulse schemes of the reverse INEPT are shown, with a full INEPT delay without any modifications ($\tau_2 = 1/2J$, black), a shortened INEPT delay ($\tau_2 < 1/2J$, blue) and an INEPT delay shortened by delayed decoupling ($\tau_2 < 1/2J$, $\tau_{ddc} = 1/2J - \tau_2$, red). (B) FIDs resulting from the pulse sequences with the corresponding colour using $R_2 = 200\ s^{-1}$ and $^1J_{CH} = 147$ Hz. For the latter two cases (blue and red), τ_2 was shortened to 1.4 ms and τ_{ddc} was consequently 2 ms (red). The small arrow indicates the point of the FID when the signal-to-noise value reaches 1 in this simulation. The nontypical shape of the FID in experiments with delayed decoupling results from the continued transfer of magnetisation after the start of the acquisition. (C) Overlay of the Fourier transforms of the corresponding FIDs from (B), highlighting the sensitivity increase achieved by delayed decoupling (freq. = frequency).

The shape of the FID and the Fourier transformed signal are reminiscent of sharpening window functions.[34,42] However, the important difference is that with such processing window functions the noise is increased, leading to lower sensitivity. In contrast, with delayed decoupling, the noise stays constant and only the signal is increased.

The unusual shape of the FID can potentially lead to artefacts in the Fourier-transformed signal. In the direct dimension, negative shoulders can arise for sharp signals of buffer substances or flexible moieties of biomolecules. These artefacts can be eliminated by applying a window function with the form $1/\sin(\pi J_{CH}\tau)$ to the first few points of the FID, compensating for the magnetisation transfer during τ_{ddc} (Figure S2). The window function slightly decreases the signal-to-noise ratio for slowly relaxing signals ($\approx 5\%$), as it increases the noise of the first few points in the FID. This compensating window function has been implemented in a python processing script for the software TopSpin (included in the supplementary material). The parameters for the window function are automatically determined from the NMR experiment and the function is generated on-the-fly and applied to the FID before the main apodization as defined in the processing parameters is carried out. However, for most experiments this correction did not have to be applied because the signals of interest were broad and did not display visible artefacts.

Delayed decoupling therefore represents a simple means to improve sensitivity for fast relaxing signals, which can readily be implemented in a multitude of NMR experiments.

Optimisation of INEPT and recovery delays by empirical search

The lengths of forward INEPT, reverse INEPT and the recovery delay were optimised by an empirical search using a test protein, the fully protonated Metε-[$^{13}CH_3$] labelled homoheptameric 11S proteasome activator from *Trypanosoma brucei*[43] ($11S_7$). The $11S_7$ complex has a molecular weight of 175 kDa and is in the size range of an antibody (150 kDa) or a membrane protein within a micelle (100–150 kDa). Therefore, the $11S_7$ complex is a reasonable surrogate protein for the optimisation of the XL-ALSOFAST-HMQC.

Optimisation was performed by testing an array of different combinations of forward INEPT, reverse INEPT and recovery delay lengths (6·6·3 = 108 points). The signal-to-noise values for the methionine methyl signals were determined for every experiment and analysed (for details see supplementary material). Results for a structured (S) and a flexible (F) methyl group can be seen in Figure 4. For methyl groups in the structured regions of the protein, the optimal length of the INEPT delays strongly deviates from the 3.4 ms that are theoretically expected for a full magnetisation transfer. The fit indicates best signal-to-noise ratios for a recovery delay of 500 ms with a forward INEPT delay of 2.2 ms and a reverse INEPT delay of 1.3 ms with delayed decoupling. This optimization of the delays increased the signal-to-noise ratio by a factor of 2.4 for a structured methionine methyl group compared to an experiment with non-shortened INEPT delays (3.4 ms) and a d_1 of 1000 ms.

The maximum of the fitted function for a structured methionine residue appears to be rather flat, indicating that this optimisation does not need to be performed for every single protein of interest and that the obtained values in this study are robust and transferable to a large set of high molecular weight systems. Most XL-ALSOFAST experiments in this study have been performed with $d_1 = 500$ ms using forward and reverse INEPT delays of 2.6 ms and 1.4 ms, respectively.

The gain in sensitivity for the XL-ALSOFAST-HMQC is not the same for every signal as can be seen for a flexible and a structured methyl group in the example of the $11S_7$ complex (Figure 4B), and also in the overview given in Figure 5. It is strongly depending on the relaxation experienced by the individual groups and fast relaxing signals benefit most from the modifications introduced in the XL-ALSOFAST-HMQC. Interestingly, also for rather flexible moieties, the XL-ALSOFAST-HMQC seems to increase sensitivity, as opposed to for example, [^{15}N,^{1}H]-TROSY, where signals of flexible groups have reduced intensity.

Data obtained at two B_0-fields (700 and 900 MHz) showed no significant field dependence of the sensitivity enhancement of the XL-ALSOFAST experiment (< 5 % difference). This is in line with theory, as the exploited effects, that is, methyl-TROSY, cross-relaxation and J-coupling, are field independent or approximately so.

The analysis of this extensive dataset allowed us to determine the relative contributions of the modifications applied to the forward and reverse INEPT to the overall sensitivity improvement of 2.4. For the structured signal S in the $11S_7$ complex, delayed decoupling leads to an increase in sensitivity of a factor 2.1, which translates into a more than 4-fold reduction in measurement time. Note however, that due to the symmetry of the gs-XL-ALSOFAST experiment, shortening of τ_2 leads to an overall reduction of the length of the pulse sequence by $2\tau_2$. Regarding the forward INEPT, the

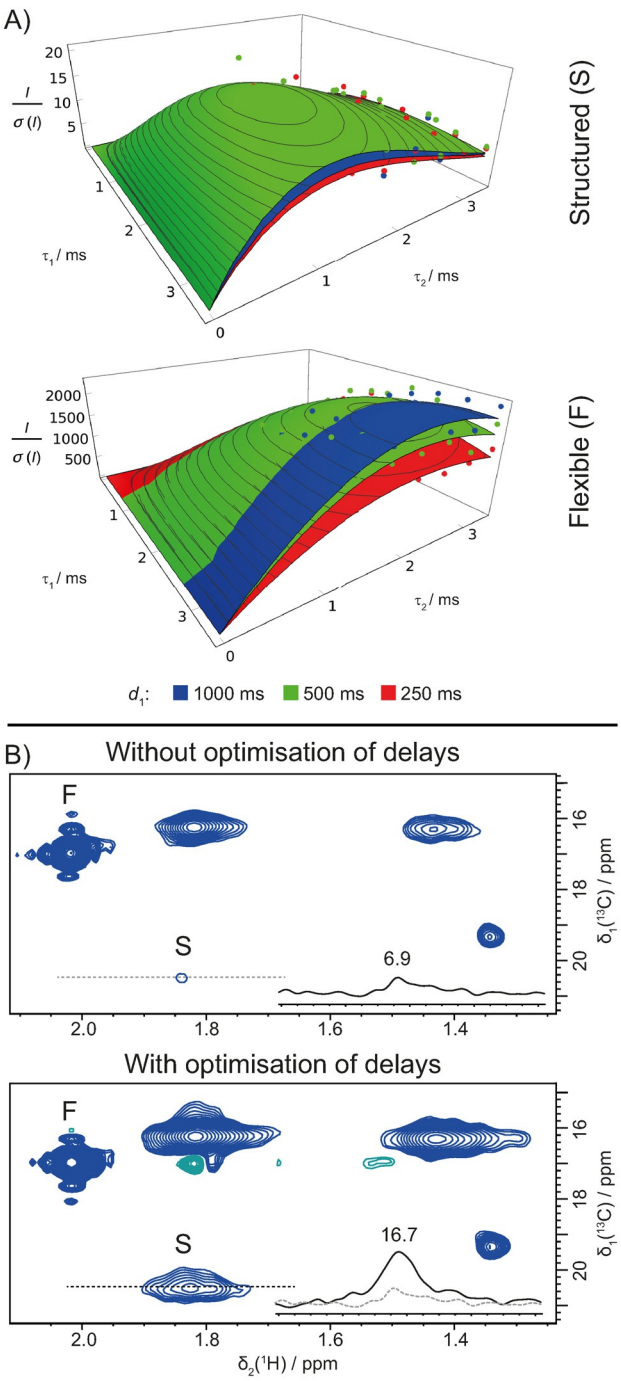

Figure 4. Results of the empirical search for the optimal lengths of recovery delay (d_1), as well as the forward (τ_1) and reverse (τ_2) INEPT delays. (A) A matrix of different durations of the delays d_1, τ_1 and τ_2 was recorded on the fully protonated Metε-[^{13}CH$_3$] labelled 175 kDa $11S_7$ complex and signal-to-noise ratios (I/σ_I) were determined for each signal. The data of each series with constant d_1 were fitted separately (coloured planes, see supplementary material) and are shown for two selected residues with different flexibility. The signal from a structured methionine residue (S) has maximal sensitivity with $d_1 = 500$ ms for τ_1 and τ_2 of 2.2 ms and 1.3 ms, respectively. B) Comparison between a non-optimised ($d_1 = 1000$ ms, $\tau_1 = \tau_2 = 3.4$ ms) and the optimised gs-XL-ALSOFAST-HMQC ($d_1 = 500$ ms, $\tau_1 = 2.6$ ms, $\tau_2 = 1.4$ ms). Signals of structured methionine residues benefit largely from the modifications. The presented 1D slices were extracted for the methionine S. Numbers over the 1D slice indicate signal-to-noise ratios. The spectra were obtained at 298 K on a Bruker 700 MHz AVNEO instrument equipped with a TCI cryoprobe using a 75 μM $11S_7$ sample in a 3 mm tube.

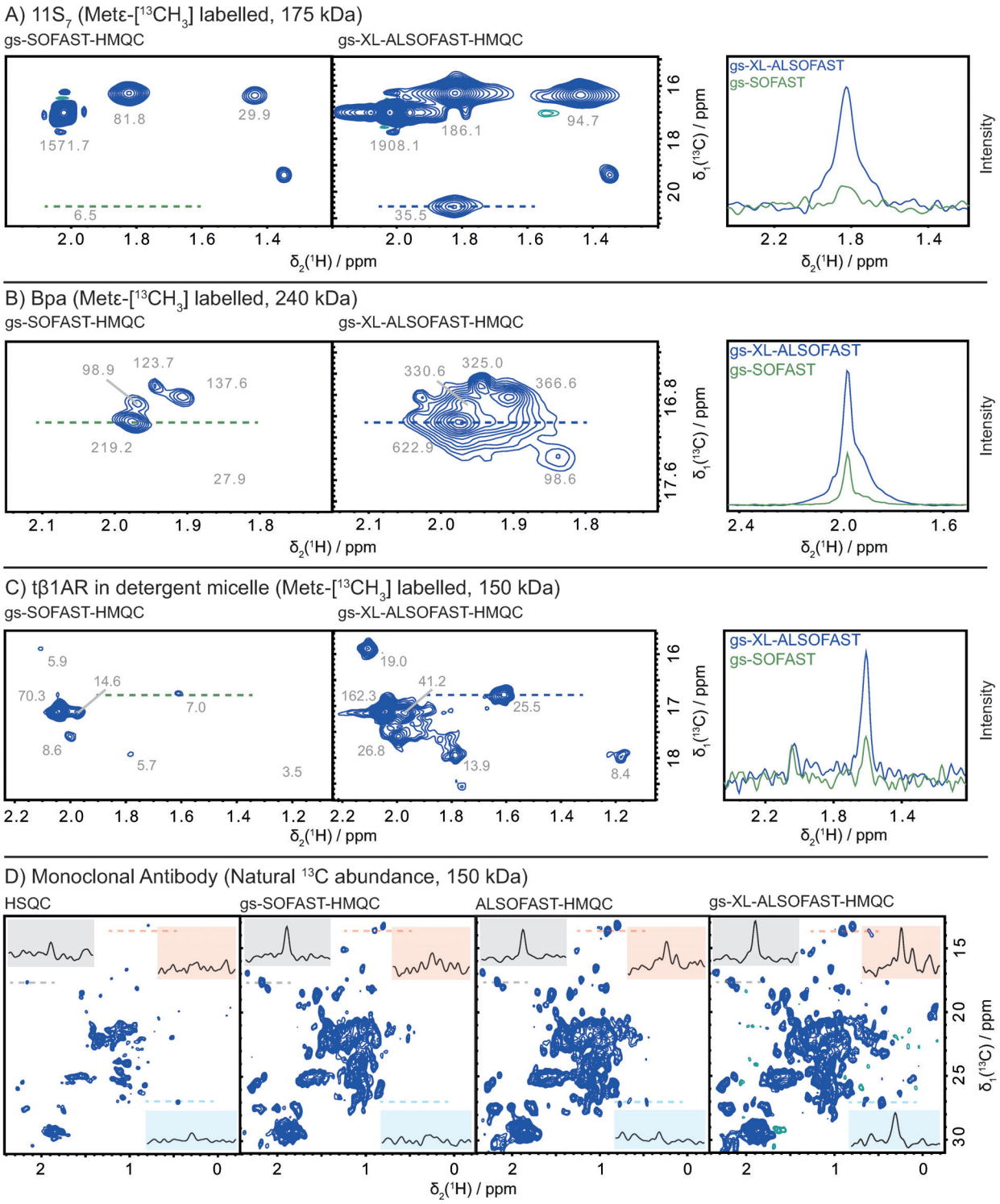

Figure 5. A) to C) Comparison between the gs-SOFAST-HMQC and the gs-XL-ALSOFAST-HMQC. The panel on the right shows 1D slices of selected signals indicated by dotted lines of corresponding colour in the HMQC. Grey numbers indicate signal-to-noise ratios for adjacent peaks. The gs-XL-ALSOFAST usually increases the sensitivity of the experiment by a factor between 2 and 3. All spectra were recorded on 5 mm TCI cryoprobes using 3 mm NMR sample tubes. (A) Spectra of a 75 μM $11S_7$ sample (500 μM monomer concentration), recorded in 1 h at 298 K on a 900 MHz spectrometer. Forward and reverse INEPT delay lengths were 2.6 ms and 1.4 ms, respectively. (B) 33 μM Bpa sample (400 μM monomer concentration), recorded in 22 h in the same way as in (A) but with forward and reverse INEPT delays of 1.5 ms and 1.4 ms, respectively. (C) 50 μM tβ1AR sample recorded in 3.5 h as in (A) but on a 700 MHz spectrometer. Note that the performance of the XL-ALSOFAST experiment is essentially independent of the B_0-field strength. (D) Fingerprint spectra of the methyl region of a monoclonal antibody (40 mg mL^{-1}) at natural isotope abundance. Same parameters as in (A) were used for the measurement, except that the temperature was 323 K and the spectra were recorded in 10 h. Slices of selected signals are shown and correspond to the equally coloured line in the 2D spectrum.

parameters d_1 and τ_1 are interdependent and lead to a combined gain in sensitivity of 1.2. However, when the XL-ALSOFAST is compared to other experiments, the factor contributed by d_1 and τ_1 can exceed a value of 1.7, due to the more selective excitation and better preservation of non-observed magnetisation, as discussed later.

Superior artefact suppression by aligning unwanted magnetization along the +z-axis

The ALSOFAST approach has an intrinsic advantage when it comes to suppression of unwanted (not ^{13}C bound) signals: non-observed magnetisation is aligned along the $+z$-axis at the start of acquisition. Therefore, only the fraction of signals ending up off the z-axis due to pulse imperfections contributes to artefactual NMR signals. If additional gradient selection (gs) is implemented as in the gs-XL-ALSOFAST used throughout this work, artefacts from non-labelled moieties are essentially eliminated.

We submitted artefact suppression to stringent tests with the following demanding samples: a membrane protein sample, where detergent molecules are in 100-fold excess over the protein signals; a formulated therapeutic antibody at natural ^{13}C-abundance, where non-labelled groups of the antibody are in 100-fold excess and excipients are present in even higher excess; and a sample of the small protein PCuC[44] containing non-deuterated buffer substances (i.e. MOPS) at 50 mM concentration. In all these samples, spurious signals are very nicely suppressed and no noise bands are visible. Such t_1-noise is particularly harmful for non-uniform sampling (NUS) approaches,[45,46] where noise bands are typically exaggerated by non-continuous sampling. With the gs-XL-ALSOFAST experiment at 25% NUS, no noise bands appeared even in presence of 50 mM MOPS buffer (Figure S3). Such potential artefacts could further be reduced by selective excitation of only the region of interest in the ^{13}C dimension, thus avoiding folding of buffer signals into the spectral window.[38,47]

In summary, artefact suppression in the XL-ALSOFAST approach is superior to most other experiments, since only a small fraction of non-wanted magnetisation remains off the $+z$-axis, and these small residual coherences are effectively suppressed by pulsed field gradients. Clean spectra, as produced from this experiment allow detailed analysis of signals close to buffer signals and are ideally suited for automated statistical analysis as used for example, for quality assessment of clinical antibodies.

Expanding the range of biological systems accessible to NMR spectroscopy

The high sensitivity of the XL-ALSOFAST approach combined with excellent artefact suppression allows now to expand the range of biological systems that can be studied by NMR. Since deuteration is not required, high molecular weight proteins and complexes can be studied that originate from mammalian expression hosts which do not yet allow the production of highly deuterated samples. Since numerous proteins can only be produced by such hosts, these systems will greatly benefit from this improved experiment. Spectra of the fully protonated and detergent solubilised thermostabilised β_1 adrenergic receptor from turkey (tβ1AR) highlight this application for a protein produced in HEK293 cells.[48] On this sample, the gs-XL-ALSOFAST-HMQC has up to three-fold higher sensitivity than the gs-SOFAST-HMQC, which is considered the state-of-the-art for such samples. We thus were able to record a spectrum of this membrane protein in 45 minutes (Figure S5), which opens the way for studying more native-like constructs of inherently unstable GPCRs.

In general, the XL-ALSOFAST approach allows the measurement of high molecular weight systems without the need for expensive deuteration. The possibilities for studies of fully protonated high molecular weight complexes can be seen in methyl spectra of the $11S_7$ complex (175 kDa, Figure 5A) and the homododecameric bacterial proteasome activator from *Mycobacterium tuberculosis*[49] (Bpa, 240 kDa, Figure 5B).

Additionally, the high sensitivity of the gs-XL-ALSOFAST allows to record spectra of unstable proteins at low concentrations. The increased sensitivity of the experiment enables the reduction of measurement time by a factor of up to 9 compared to currently used experiments under the same conditions, thus being useful for the acquisition of NMR data on unstable complexes.

Higher order structure analysis on therapeutic antibodies

An important emerging application of NMR in the pharmaceutical industry is the quality control of biological therapeutics, like monoclonal antibodies (150 kDa), by measurement of methyl spectra at natural isotope abundance.[18–20,37] The ability to cope with fully protonated high molecular weight systems and at the same time allowing excellent suppression of artefacts makes the gs-XL-ALSOFAST-HMQC the ideal experiment for this application. We compared the performance of several experiments on a monoclonal antibody solution (40 mg mL^{-1}) at 323 K (Figure 5D) and evaluated signal-to-noise ratios for selected peaks in the obtained fingerprint spectra. The XL-ALSOFAST-HMQC has a higher sensitivity than the currently proposed HSQC experiments by a factor of 2–3. In comparison to the SOFAST-HMQC, the ALSOFAST approach allows for the observation of resonances in a larger spectral window, as it is not limited by the bandwidth of the selective pulses needed in the SOFAST scheme. Therefore, overall, the XL-ALSOFAST-HMQC is the best-suited experiment for recording spectra of biological therapeutics as it combines best artefact suppression with highest sensitivity.

Conclusion

In this work, we presented the XL-ALSOFAST-[^{13}C,^{1}H]-HMQC, which is optimized for non-deuterated high molecular weight systems and can yield sensitivity improvements up

to a factor of five. Improved sensitivity is achieved by shortening the pulse sequence, while avoiding otherwise inevitable losses due to incomplete magnetisation transfer. To this end, we introduce the concept of delayed decoupling, which increases sensitivity for fast relaxing signals by a simple modification of the pulse sequence: during acquisition, *J*-coupling evolution is allowed to proceed until maximal magnetisation transfer is achieved before decoupling is started. This leads to more intense and longer-lasting NMR signals.

We show representative examples of biomolecular complexes ranging from 100 to 240 kDa in molecular mass, where sensitivity enhancements of typically factor three were observed for strongly relaxing signals, translating into nine-fold reduction in measurement time compared to standard approaches. Such short measurement times might enable NMR studies of inherently unstable proteins like many GPCRs. Among the studied samples the integral membrane protein tβ1AR and a therapeutic antibody are noteworthy, as they were produced in human and hamster cell lines, where deuteration is presently not feasible. However, there is an increasing number of protocols to label methyl groups with ^{13}C in protonated background. In combination with the XL-ALSOFAST, therefore, large proteins and protein complexes, which were formerly inaccessible to NMR, can now be studied at the atomic level.

Furthermore, with samples, where unlabeled substances are present in high excess (detergents, buffer, unlabeled protein signals) superior artefact suppression could be shown. This highlights the potential of the XL-ALSOFAST approach with gradient selection for studying higher order structure of therapeutic antibodies, and also for future in-cell studies.

We therefore trust that the XL-ALSOFAST approach together with the concept of delayed decoupling—for which applications are not limited to this experiment—will expand the range of biomolecular systems accessible to NMR spectroscopy.

Acknowledgements

We are very grateful to Silke Wiesner for providing plasmid DNA for the 11S proteasome activator and to Tatjana von Rosen from Eilika Weber-Ban's group and Fabia Canonica from Rudi Glockshuber's group for kindly providing the Bpa and PCuC samples, respectively. We thank Gebhard F.X. Schertler for providing a stable HEK293S cell line to produce tβ1AR and Ching-Ju Tsai for valuable support during its purification. We are thankful to Burkhard Luy for sharing insights into gradient selection procedures and to Frank Löhr for spotting an error in an earlier version of the pulse sequence. We are indebted to Yaroslav Nikolaev for accelerating data evaluation by providing a Matlab script and to Peter Güntert for sharing a copy of the software PROSA.[50] Finally, we would like to thank Simon H. Rüdisser, Fred F. Damberger, Alfred Ross, Wolfgang Bermel, Helena Kovacs and Wolfgang Jahnke for inspiring discussions and help on many aspects of this work. This project was funded by SNSF grant 31003A_179319.

Conflict of interest

The authors declare no conflict of interest.

Keywords: delayed decoupling · isotopic labeling · NMR spectroscopy · proteins · XL-ALSOFAST

[1] A. R. Aricescu, R. Assenberg, R. M. Bill, D. Busso, V. T. Chang, S. J. Davis, A. Dubrovsky, L. Gustafsson, K. Hedfalk, U. Heinemann, et al., *Acta Crystallogr. Sect. D* **2006**, *62*, 1114–1124.
[2] R. Assenberg, P. T. Wan, S. Geisse, L. M. Mayr, *Curr. Opin. Struct. Biol.* **2013**, *23*, 393–402.
[3] E. A. McKenzie, W. M. Abbott, *Methods* **2018**, *147*, 40–49.
[4] D. P. Frueh, A. C. Goodrich, S. H. Mishra, S. R. Nichols, *Curr. Opin. Struct. Biol.* **2013**, *23*, 734–739.
[5] M. P. Foster, C. A. McElroy, C. D. Amero, *Biochemistry* **2007**, *46*, 331–340.
[6] Y. Kofuku, T. Ueda, J. Okude, Y. Shiraishi, K. Kondo, M. Maeda, H. Tsujishita, I. Shimada, *Nat. Commun.* **2012**, *3*, 1045.
[7] Y. Kofuku, T. Ueda, J. Okude, Y. Shiraishi, K. Kondo, T. Mizumura, S. Suzuki, I. Shimada, *Angew. Chem. Int. Ed.* **2014**, *53*, 13376–13379; *Angew. Chem.* **2014**, *126*, 13594–13597.
[8] R. Nygaard, Y. Zou, R. O. Dror, T. J. Mildorf, D. H. Arlow, A. Manglik, A. C. Pan, C. W. Liu, J. J. Fung, M. P. Bokoch, et al., *Cell* **2013**, *152*, 532–542.
[9] R. Horst, J. J. Liu, R. C. Stevens, K. Wüthrich, *Angew. Chem. Int. Ed.* **2013**, *52*, 10762–10765; *Angew. Chem.* **2013**, *125*, 10962–10965.
[10] S. Isogai, X. Deupi, C. Opitz, F. M. Heydenreich, C.-J. Tsai, F. Brueckner, G. F. X. Schertler, D. B. Veprintsev, S. Grzesiek, *Nature* **2016**, *530*, 237–241.
[11] A. S. Solt, M. J. Bostock, B. Shrestha, P. Kumar, T. Warne, C. G. Tate, D. Nietlispach, *Nat. Commun.* **2017**, *8*, 1795.
[12] M. T. Eddy, M. Y. Lee, Z. G. Gao, K. L. White, T. Didenko, R. Horst, M. Audet, P. Stanczak, K. M. McClary, G. W. Han, et al., *Cell* **2018**, *172*, 68–80.
[13] J. N. Frei, R. W. Broadhurst, M. J. Bostock, A. Solt, A. J. Y. Jones, F. Gabriel, A. Tandale, B. Shrestha, D. Nietlispach, *Nat. Commun.* **2020**, *11*, 699.
[14] I. Shimada, T. Ueda, Y. Kofuku, M. T. Eddy, K. Wüthrich, *Nat. Rev. Drug Discovery* **2019**, *18*, 59–82.
[15] C. R. Sanders, F. Sönnichsen, *Magn. Reson. Chem.* **2006**, *44*, S24–S40.
[16] R. D. Krueger-Koplin, P. L. Sorgen, S. T. Krueger-Koplin, I. O. Rivera-Torres, S. M. Cahill, D. B. Hicks, L. Grinius, T. A. Krulwich, M. E. Girvin, *J. Biomol. NMR* **2004**, *28*, 43–57.
[17] J. M. Glück, M. Wittlich, S. Feuerstein, S. Hoffmann, D. Willbold, B. W. Koenig, *J. Am. Chem. Soc.* **2009**, *131*, 12060–12061.
[18] L. W. Arbogast, R. G. Brinson, J. P. Marino, *Anal. Chem.* **2015**, *87*, 3556–3561.
[19] L. W. Arbogast, R. G. Brinson, J. P. Marino, *Methods Enzymol.* **2016**, *566*, 3–34.
[20] R. G. Brinson, J. P. Marino, F. Delaglio, L. W. Arbogast, R. M. Evans, A. Kearsley, G. Gingras, H. Ghasriani, Y. Aubin, G. K. Pierens, et al., *MAbs* **2019**, *11*, 94–105.
[21] F. Casagrande, K. Dégardin, A. Ross, *J. Biomol. NMR* **2020**.
[22] J. Fiaux, E. B. Bertelsen, A. L. Horwich, K. Wüthrich, *J. Biomol. NMR* **2004**, *29*, 289–297.
[23] R. Sprangers, L. E. Kay, *Nature* **2007**, *445*, 618–622.
[24] D. M. LeMaster, *Methods Enzymol.* **1989**, *177*, 23–43.
[25] K. Pervushin, R. Riek, G. Wider, K. Wüthrich, *Proc. Natl. Acad. Sci. USA* **1997**, *94*, 12366–12371.
[26] V. Tugarinov, L. E. Kay, *J. Biomol. NMR* **2004**, *29*, 369–376.
[27] B. Franke, C. Opitz, S. Isogai, A. Grahl, L. Delgado, A. D. Gossert, S. Grzesiek, *J. Biomol. NMR* **2018**, *71*, 173–184.

[28] L. Skora, B. Shrestha, A. D. Gossert, *Methods Enzymol.* **2015**, *565*, 245 – 288.
[29] A. Sitarska, L. Skora, J. Klopp, S. Roest, C. Fernández, B. Shrestha, A. D. Gossert, *J. Biomol. NMR* **2015**, *62*, 191 – 197.
[30] C. Opitz, S. Isogai, S. Grzesiek, *J. Biomol. NMR* **2015**, *62*, 373 – 385.
[31] K. Pervushin, *Q. Rev. Biophys.* **2000**, *33*, 161 – 197.
[32] S. Schütz, R. Sprangers, *Prog. Nucl. Magn. Reson. Spectrosc.* **2020**, *116*, 56 – 84.
[33] P. Schanda, E. Kupĉe, B. Brutscher, *J. Biomol. NMR* **2005**, *33*, 199 – 211.
[34] J. Cavanagh, W. J. Fairbrother, A. G. Palmer III, N. J. Skelton, M. Rance, *Protein NMR Spectroscopy: Principles and Practice*, Academic Press, San Diego, **2010**.
[35] J. Cavanagh, A. G. Palmer, P. E. Wright, M. Rance, *J. Magn. Reson.* **1991**, *91*, 429 – 436.
[36] L. E. Kay, P. Keifer, T. Saarinen, *J. Am. Chem. Soc.* **1992**, *114*, 10663 – 10665.
[37] L. W. Arbogast, F. Delaglio, J. R. Tolman, J. P. Marino, *J. Biomol. NMR* **2018**, *72*, 149 – 161.
[38] L. Mueller, *J. Biomol. NMR* **2008**, *42*, 129 – 137.
[39] D. Schulze-Sünninghausen, J. Becker, M. R. M. Koos, B. Luy, *J. Magn. Reson.* **2017**, *281*, 151 – 161.
[40] D. Braun, K. Wüthrich, G. Wider, *J. Magn. Reson.* **2003**, *165*, 89 – 94.
[41] R. R. Ernst, W. A. Anderson, *Rev. Sci. Instrum.* **1966**, *37*, 93 – 102.
[42] R. R. Ernst, G. Bodenhausen, A. Wokaun, *Principles of Nuclear Magnetic Resonance in One and Two Dimensions*, Oxford University Press, Oxford, **1990**.
[43] A. Förster, E. I. Masters, F. G. Whitby, H. Robinson, C. P. Hill, *Mol. Cell* **2005**, *18*, 589 – 599.
[44] F. Canonica, D. Klose, R. Ledermann, M. M. Sauer, H. K. Abicht, N. Quade, A. D. Gossert, S. Chesnov, H. M. Fischer, G. Jeschke, et al., *Sci. Adv.* **2019**, *5*, eaaw8478.
[45] J. C. Hoch, *Methods Enzymol.* **1989**, *176*, 216 – 241.
[46] S. Robson, H. Arthanari, S. G. Hyberts, G. Wagner, *Methods Enzymol.* **2019**, *614*, 263 – 291.
[47] H. Geen, R. Freeman, *J. Magn. Reson.* **1991**, *93*, 93 – 141.
[48] P. J. Reeves, J. M. Kim, H. G. Khorana, *Proc. Natl. Acad. Sci. USA* **2002**, *99*, 13413 – 13418.
[49] M. Bolten, C. L. Delley, M. Leibundgut, D. Boehringer, N. Ban, E. Weber-Ban, *Structure* **2016**, *24*, 2138 – 2151.
[50] P. Güntert, V. Dötsch, G. Wider, K. Wüthrich, *J. Biomol. NMR* **1992**, *2*, 619 – 629.

Manuscript received: May 29, 2020
Accepted manuscript online: August 3, 2020
Version of record online: August 26, 2020

